Prepublished copy

Nature Environment & Pollution Technology

This is a peer-reviewed prepublished version of the paper to be published in Vol. 25, No. 2, June 2026 issue

Synthesis of a Novel Activated Carbon/ZnO Nanocomposite from the Dead Bark of Indian Jujube for Efficient Removal of Cationic Dye Pollutant

Rekha Sharma[1], Bhanupriya Mordhiya[1]†, Parmeshwar Lal Meena[1], Pooja Meena[1] and Surendra Dutt Arya[2]

[1]Department of Chemistry, University of Rajasthan, Jaipur, Rajasthan, India

[2]Saras Dairy, Jaipur, Rajasthan, India

†Corresponding Author: Bhanupriya Mordhiya; bmordhiya@gmail.com

ORCID ID: 0000-0003-4450-2814

Key Words	Activated carbon, ZnO nanocomposite, *Ziziphus mauritiana*, Toluidine blue, Adsorption, Wastewater treatment
DOI	https://doi.org/10.46488/NEPT.2026.v25i02.B4383 (DOI will be active only after the final publication of the paper)
Citation for the Paper	Sharma, R., Mordhiya, B., Meena, P. L., Meena, P. and Arya, S. D. 2026. Synthesis of a novel activated carbon/ZnO nanocomposite from the dead bark of Indian Jujube for efficient removal of cationic dye pollutant. *Nature Environment and Pollution Technology*, 25(2), B4383. https://doi.org/10.46488/NEPT.2026.v25i02.B4383

ABSTRACT

In this study, a novel activated carbon/zinc oxide (AC/ZnO) nanocomposite was synthesized from the dead bark of *Ziziphus mauritiana* (Indian jujube) through chemical activation and high-temperature treatment. The nanocomposite was characterized using FTIR, XRD, BET, FESEM, TEM, XPS, and zeta potential analyses, confirming its porous structure and ZnO incorporation. Batch adsorption experiments were performed to evaluate its ability to remove toluidine blue (TB) dye from aqueous solutions. Under optimized conditions (0.04 g of adsorbent in 100 mL of dye solution at pH 11.5, a contact time of 50 min, and 25 ± 2°C), the nanocomposite achieved a maximum removal efficiency of 99.6% and an adsorption capacity

of 49.9 $mg.g^{-1}$. The adsorption process followed the Langmuir isotherm model and pseudo-second-order kinetics, indicating a monolayer chemisorption mechanism. Thermodynamic parameters confirmed that the process is spontaneous and endothermic. The nanocomposite retained over 90% efficiency after four regeneration cycles, demonstrating stability and reusability. These findings highlight the potential of *Z. mauritiana*-derived AC/ZnO as a sustainable and cost-effective adsorbent for dye removal from wastewater.

INTRODUCTION

Water contamination by synthetic dyes has become a global environmental challenge due to their complex aromatic structures, high stability, and resistance to biodegradation. Large volumes of colored effluents are released daily from textile, leather, paper, paint, cosmetics, and pharmaceutical industries, leading to severe ecological and health impacts (Hu et al., 2025; Maheshwari et al., 2021; Hambisa et al., 2022). Once discharged into aquatic systems, dyes reduce dissolved oxygen, hinder photosynthesis, and can bioaccumulate through the food chain, posing mutagenic and carcinogenic risks to living organisms (Ahmad et al., 2020; Jani et al., 2022). Conventional wastewater treatment methods, such as coagulation–flocculation, oxidation, and biological degradation, are either cost-intensive, produce large amounts of sludge, or exhibit limited efficiency in achieving complete dye removal (Khazaal et al., 2022; Nath et al., 2018). Therefore, there is a pressing need for sustainable and efficient adsorbents to address dye pollution.

Among the various treatment methods, adsorption has emerged as a promising technique because of its simplicity, cost-effectiveness, and high efficiency in removing dyes from water (Akhtar et al., 2025). Activated carbon (AC) remains the most widely used adsorbent due to its large surface area, tunable porosity, and active surface functionalities (Luo et al., 2019). However, the commercial production of AC relies on non-renewable precursors and incurs high costs, restricting its large-scale application (Abo El Naga et al., 2019). To overcome this

limitation, researchers have explored low-cost and renewable precursors such as agricultural residues, fruit peels, seeds, and industrial by-products (Shrivastva et al., 2022; Deshmukh et al., 2022; Gupta et al., 2025). Furthermore, hybrid nanocomposites, where AC is combined with metal oxides (e.g., ZnO, TiO_2, MnO_2), have attracted attention due to their enhanced surface activity, stability, and adsorption capacity (Nguyen et al., 2020; Mordhiya et al., 2024). Despite these advances, the specific utilization of woody biomass and bark-based residues remains underexplored. Most studies have focused on seeds, cores, or shells (Bouchelkia et al., 2023; Malika et al., 2021; Venkatesan et al., 2024), while dead bark materials are often discarded as waste despite being lignocellulose-rich precursors suitable for high-quality activated carbon. To the best of our knowledge, no prior reports exist on the synthesis of AC/ZnO nanocomposites using *Ziziphus mauritiana* (Indian jujube) bark. This represents a significant research gap, because Z. mauritiana is widely available in Rajasthan and other semi-arid regions of India, and its bark is usually left unused. Valorizing such biomass not only reduces environmental burden but also provides a low-cost route to prepare efficient nanocomposites.

The novelty of the present study lies in addressing this research gap by developing, for the first time, an AC/ZnO nanocomposite derived from Z. mauritiana bark. While AC/ZnO systems have been reported from other plant residues, this precursor choice has not been investigated. Our approach, therefore, combines sustainable waste valorization with the design of efficient adsorbents for the remediation of dyes.

The present work focuses on synthesizing an AC/ZnO nanocomposite from Z. mauritiana bark and systematically investigating its efficiency for removing cationic dye pollutants from aqueous solutions, using toluidine blue (TB) as a model contaminant. A comprehensive suite of characterizations was employed, including FTIR, XRD, FESEM, TEM, BET, XPS, and zeta potential analysis, to confirm the structure, morphology, and surface properties of the

nanocomposite. Batch adsorption experiments were performed to evaluate the effects of pH, adsorbent dosage, initial dye concentration, contact time, and temperature. Adsorption isotherms (Langmuir, Freundlich, Temkin, and Dubinin–Radushkevich), kinetics (pseudo-first-order, pseudo-second-order, Elovich, and intra-particle diffusion models), and thermodynamics were studied to elucidate the adsorption mechanism. Recyclability was tested over four cycles to examine reusability.

Three contributions reinforce the novelty and relevance of this work:

Sustainability: Utilization of waste biomass (Z. mauritiana bark) to produce high-quality AC/ZnO nanocomposite.

Performance: Achievement of near-complete dye removal (99.6% under optimized conditions), with adsorption capacity comparable to or better than reported biomass-based nanocomposites.

Future Feasibility: Demonstration of recyclability and acknowledgment of limitations (e.g., Zn-leaching, multi-pollutant systems) that pave the way for future investigations.

In summary, this study not only introduces a novel biomass precursor for AC/ZnO nanocomposites but also establishes the adsorption potential of the synthesized material under optimized laboratory conditions.

1. MATERIALS AND METHODS

1.1. CHEMICAL USED

The materials used in this research included zinc chloride ($ZnCl_2$), hydrochloric acid (HCl), sodium hydroxide (NaOH), distilled water, and toluidine blue (TB) dye ($C_{15}H_{14}N_3ClS$). The primary raw material employed was the dead bark of native Indian jujube. All chemicals used were of analytical grade. Toluidine blue, a heterocyclic synthetic organic dye, served as a model contaminant to simulate water pollution. With a molecular weight of 319.85 g/mol, TB is highly water-soluble and remains stable for long durations under standard temperature

conditions. Because of its propensity to be poisonous, carcinogenic, and non-biodegradable, it is a chemical that should be avoided at all costs.

1.2.PREPARATION OF NANOADSORBENT

The naturally dried bark of the *Ziziphus mauritiana* (Indian jujube) shrub was obtained locally. It was essential to eliminate any dust or pollutants that had stuck to the bark of the Indian jujube. The bark was initially chopped into small fragments and meticulously washed with tap water to remove surface contaminants, followed by rinsing with distilled water. The material underwent carbonisation by being heated in a muffle furnace at 500 °C for 2 hours. Upon cooling, the resultant black residue was pulverised into a fine powder (Sulaiman et al., 2021). To synthesise the AC/ZnO nanocomposite, one gram of *Ziziphus mauritiana* charcoal was combined with one gram of zinc chloride, and a few drops of water were incorporated to achieve a suitable paste consistency. The paste was desiccated in an oven at 80 °C for 24 hours. The dry paste was subsequently heated in a muffle furnace at 500 °C for 1 hour. Following cooling, it was subjected to multiple washes with distilled water, culminating in a final rinse with ethanol. The substance was subsequently dehydrated in an oven at 85 °C for 3 hours. The AC/ZnO nanocomposite was stored in an airtight container for subsequent characterization and utilized to examine the adsorption behavior of TB dye from aqueous solutions under various experimental conditions.

1.3.BATCH EQUILIBRIUM INVESTIGATION

The effect of several parameters, including pH, contact time, dye concentration, and adsorbent dose, on the adsorption effectiveness of the nanoadsorbent was examined using a series of batch equilibrium tests. TB dye was used as a stock solution for the experiments, which were conducted at room temperature. Dye solutions with concentrations ranging from 10 to 60 mg/L were created by diluting the stock solution. To maintain the appropriate pH levels, diluted solutions of NaOH and HCl were used to adjust the solutions to pH values of 4, 8, 10, and 11.5.

20-50 mg of nanoadsorbent were used. Adsorption kinetics, isotherms, and thermodynamic factors were studied to acquire a more profound comprehension of the adsorption mechanism. The solution was constantly stirred throughout each experiment, and once the required amount of time had passed, the mixture was centrifuged and filtered through Whatman filter paper. To measure the dye concentration, UV-Vis spectrophotometry was used. The equilibrium adsorption capacity (q_e), dye removal efficiency, and adsorption capacity (q_t) at various process phases were calculated using standard equations.

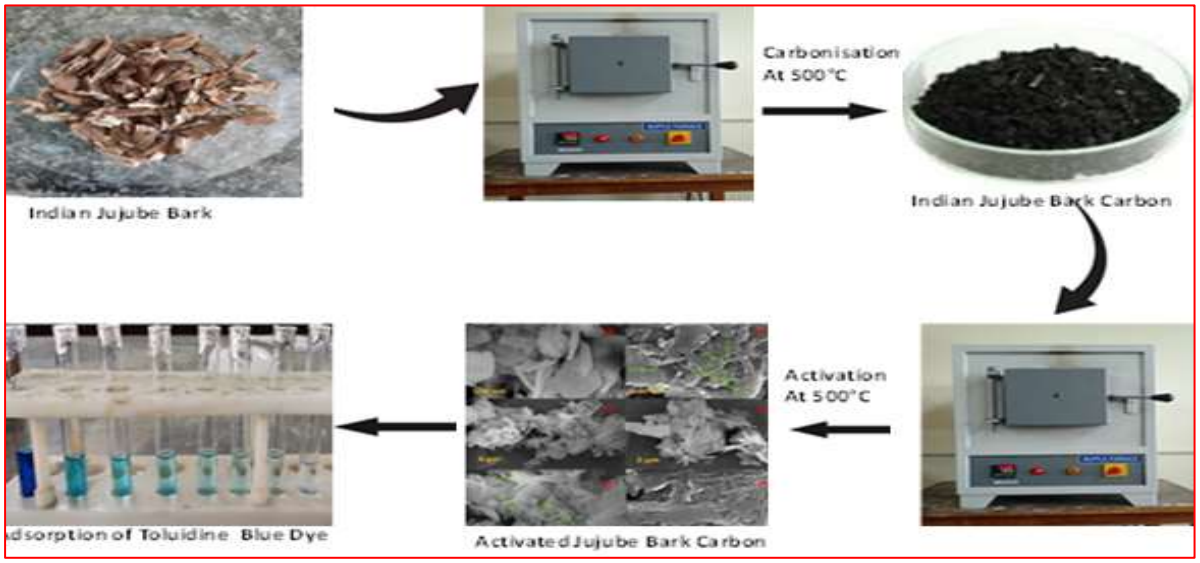

Fig.1. Schematic depiction of the pathway for the AC/ZnO nanocomposite derived from the Indian jujube dead bark.

1.4.INSTRUMENTATION

The objectives of clarifying the morphology and structure of nanoadsorbents and confirming the adsorption of dye from an aqueous solution were achieved by employing various spectroscopic techniques. The crystalline structure of nanoadsorbents is investigated using XRD techniques. The produced nanoadsorbent was subjected to XRD analysis using a PANalytical X'Pert PRO diffractometer, operating at 40 mA and 40 kV with Cu Kα radiation (λ = 1.5406 Å). To quantify the particle size and evaluate the quality of the crystalline phase, the diffraction pattern was recorded throughout a 2θ range of 10° to 80°. Furthermore, a Perkin

Elmer FTIR spectrometer operating in transmission mode was used to perform FTIR spectroscopy, scanning the range of 4000 to 400 cm^{-1}. The objectives of this analysis were to identify the functional groups on the adsorbent surface and to observe any changes in bonding properties following dye adsorption. TEM (FEI CM12) and a FESEM (Nova Nano FESEM-450 (FEI)) were used to take TEM and FESEM pictures. These pictures were taken in order to assess the adsorbent's microstructural and textural characteristics. BET examination was carried out using a surface analyser (NOVAtouch 2LX) to ascertain the material's specific surface area, pore size, and pore distribution. EDS was used to confirm the elemental makeup of the synthesised nanocomposite. The UV-Vis absorbance of the dye solutions and the adsorbent was also measured using a Shimadzu UV-2600 UV-vis spectrophotometer.

2. RESULTS AND DISCUSSIONS

2.1.CHARACTERIZATION OF NANOADSORBENT

2.1.1. XRD-BASED STRUCTURAL ANALYSIS

Fig.2 presents the XRD patterns for both pure ZnO and the AC/ZnO nanocomposite. The diffraction peaks of pure ZnO appear at 2θ values of 31.90°, 34.58°, 36.52°, 47.70°, 56.75°, 62.96°, 66.51°, 68.28°, 69.17°, 72.53°, and 77.15°, which correspond to the (100), (002), (101), (102), (110), (103), (200), (112), (201), (202), (004), and (202) planes of the hexagonal wurtzite ZnO crystal structure. In the case of the AC/ZnO composite, diffraction peaks are observed at 31.78°, 34.48°, 36.26°, 47.56°, 56.59°, 62.81°, 66.32°, 67.73°, 69.14°, 72.66°, and 77.11°, also corresponding to the same crystal planes of the hexagonal wurtzite ZnO structure. Additionally, the peaks at 2θ values of 26.65° and 44.72° are attributed to the (002) and (100) reflection planes of the hexagonal graphite structure present in the AC. (Ghaedi et al., 2012).

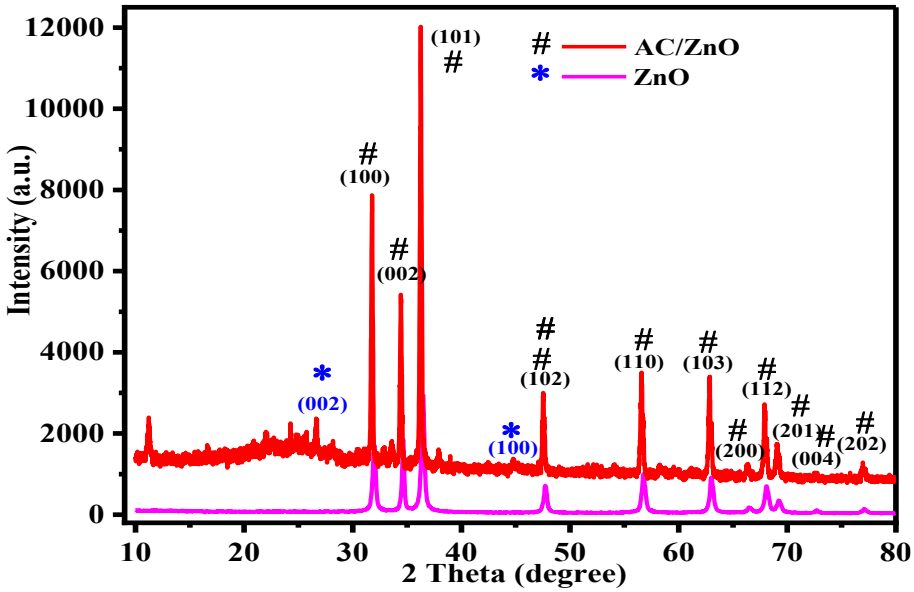

Fig. 2.XRD pattern of the pure ZnO and AC/ZnO nanocomposite

On mixing ZnO with activated carbon, the XRD peak positions related to ZnO in the composite shifted toward slightly lower 2θ values compared to pure ZnO, revealing the mixing of ZnO nanospheres with activated nanocarbon sheets. When estimating the particle size of the AC, the Debye–Scherrer relation was utilized. This was accomplished by taking into account the diffraction peak, which had a value of 2θ = 36.26°, λ = 1.5406Å, and the full width at half maximum (FWHM) (β) of the peak. A value of 61.72 nm has been determined to be the average particle size of the produced AC/ZnO nanocomposition.

2.1.2. FTIR analysis

Fig. 3 displays the FTIR spectra of the AC/ZnO nanocomposite. The peak observed at 1331 cm^{-1} corresponds to the stretching vibrations of C–C bonds found in activated carbon (Abdel-Ghani et al., 2019). A peak at 1508 cm^{-1} indicates the presence of an aromatic ring within the adsorbent. The peak at 1696 cm^{-1} is attributed to the stretching vibration of carbonyl (C=O) groups, while the 1777 cm^{-1} peak is associated with ester linkages in the nanoadsorbent (Abo El Naga et al., 2019). Bending vibrations of C–H bonds are responsible for the peaks at 2308 cm^{-1}, 2813 cm^{-1}, and 2884 cm^{-1} (Omri & Benzina, 2012). A peak at 525 cm^{-1} corresponds to the stretching vibration of the Zn–O bond, whereas pure ZnO typically shows this vibration at

570 cm^{-1}. The shift to a lower wavenumber upon incorporation with activated carbon confirms the successful integration of ZnO nanospheres into the AC nanosheets. After the dye was adsorbed onto the nanoadsorbent surface, changes in the FTIR spectrum were observed, as shown in Figure 3. A broad peak at 3314 cm^{-1} confirms the presence of alcohol groups due to O–H stretching vibrations.

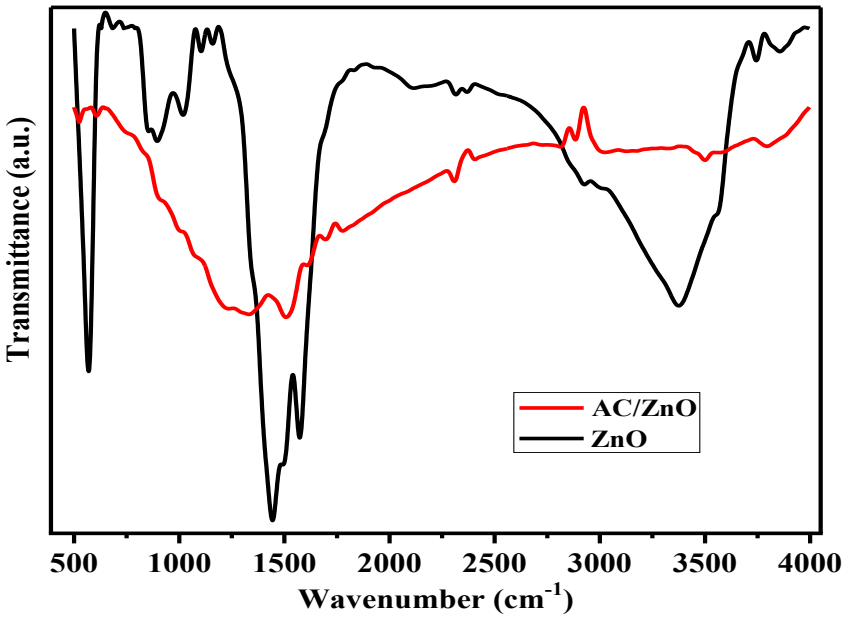

Fig.3. FTIR spectra of the pure ZnO and AC/ZnO nanoadsorbent

2.1.3. IMAGES FROM THE FESEM AND HRTEM

The presence of various elements and their distribution map along the surface of the nanoadsorbent is visible in images captured using FESEM.

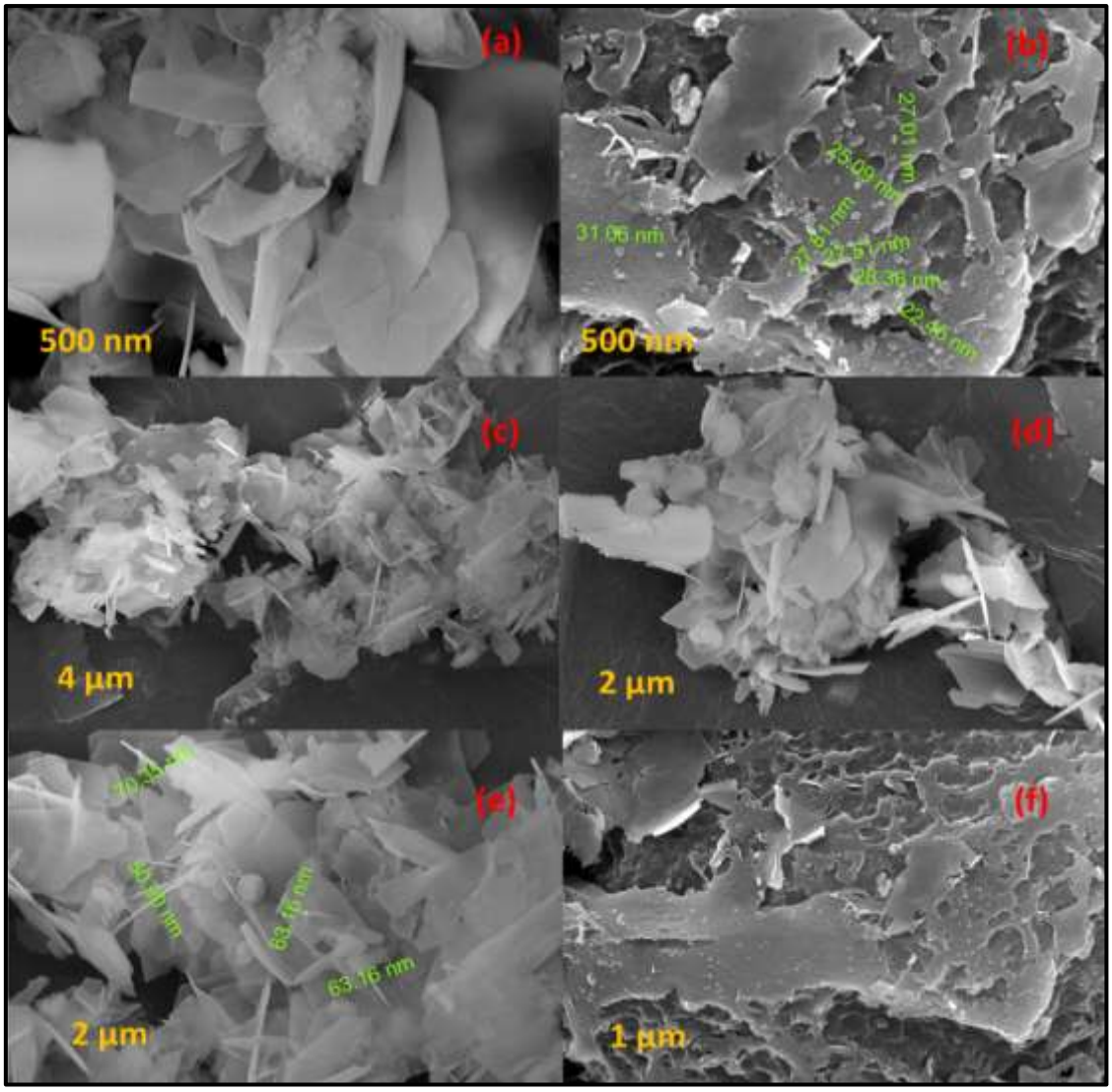

Fig.4.FESEM images of AC/ZnO nanocomposite

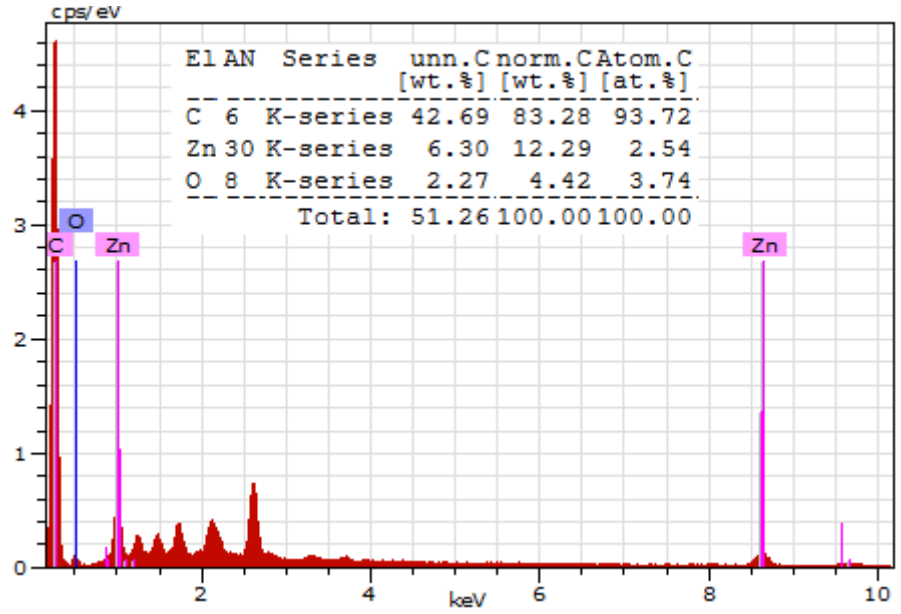

Fig.5.EDS image of AC/ZnO nanocomposite

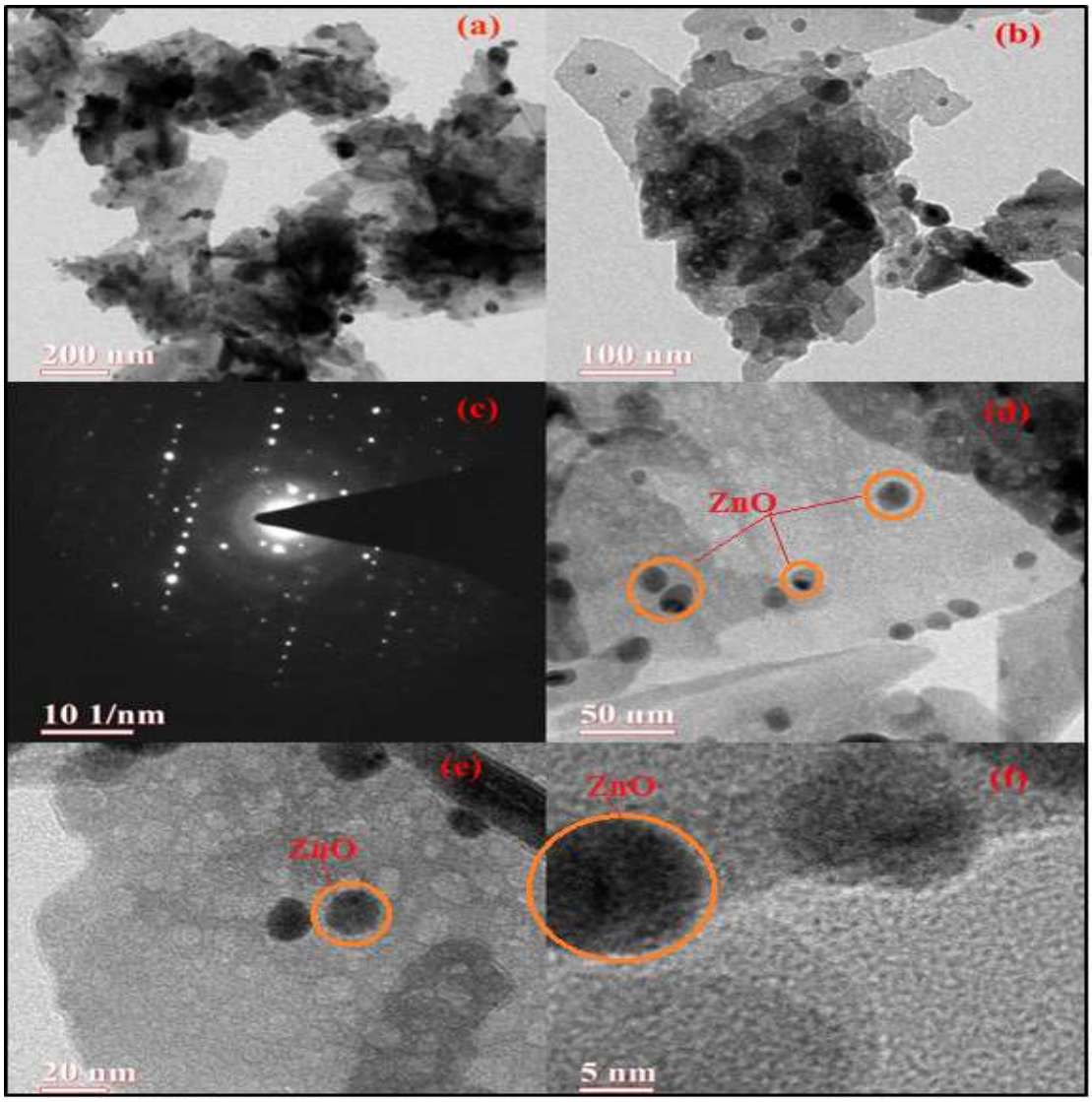

Fig.6.HRTEM images of AC/ZnO nanocomposite

Figure 4 presents the morphological analysis of the AC/ZnO nanocomposite as observed through field-emission scanning electron microscopy (FESEM). After some time has passed, images obtained from the FESEM show that there are hollow chambers surrounding the nanoadsorbent. The primary locations for adsorbing contaminants from water and removing them are housed within these hollow chambers. As these empty areas become occupied, nanoadsorbents move closer and closer to reaching peak saturation. The FESEM images provide evidence that these contaminants eventually precipitate in the hollow chambers in which they are contained. There are sticky polar interactions that occur within the hollow chambers surrounding the nanocomposite. Chelating of hazardous contaminants present in the water phase is facilitated by these sticky, polar interactions, which are responsible for binding the pollutants. Through the use of polar-polar interactions, the AC/ZnO nanocomposite enables the selective removal of contaminants from water. Due to the unequal distribution of hollow chambers around the nanoadsorbent, it may be concluded that the AC/ZnO-nanocomposite is amorphous in its natural state (Elmaguana et al., 2020). Fig. 5 displays the EDS spectrum of the AC/ZnO nanocomposite adsorbent, showing distinct peaks corresponding to the elements Zn, O, and C. Their respective weight and atomic percentages are provided in the inset table of the figure. Fig. 6 presents the TEM and HRTEM images of the synthesized AC/ZnO composite, revealing that the ZnO nanostructures have a spherical shape and are distributed across the surface of the activated carbon nanosheets. The selected area electron diffraction (SAED) pattern of the composite, shown in Fig. 6(c), features bright diffraction spots.

3.1.4. PHOTOELECTRON EMISSION SPECTRA (XPS) ANALYSIS

To obtain more information about the prepared AC/ZnO nanocomposite from the bark of Indian jujube, XPS spectra analysis was carried out, as demonstrated in Fig. 7.

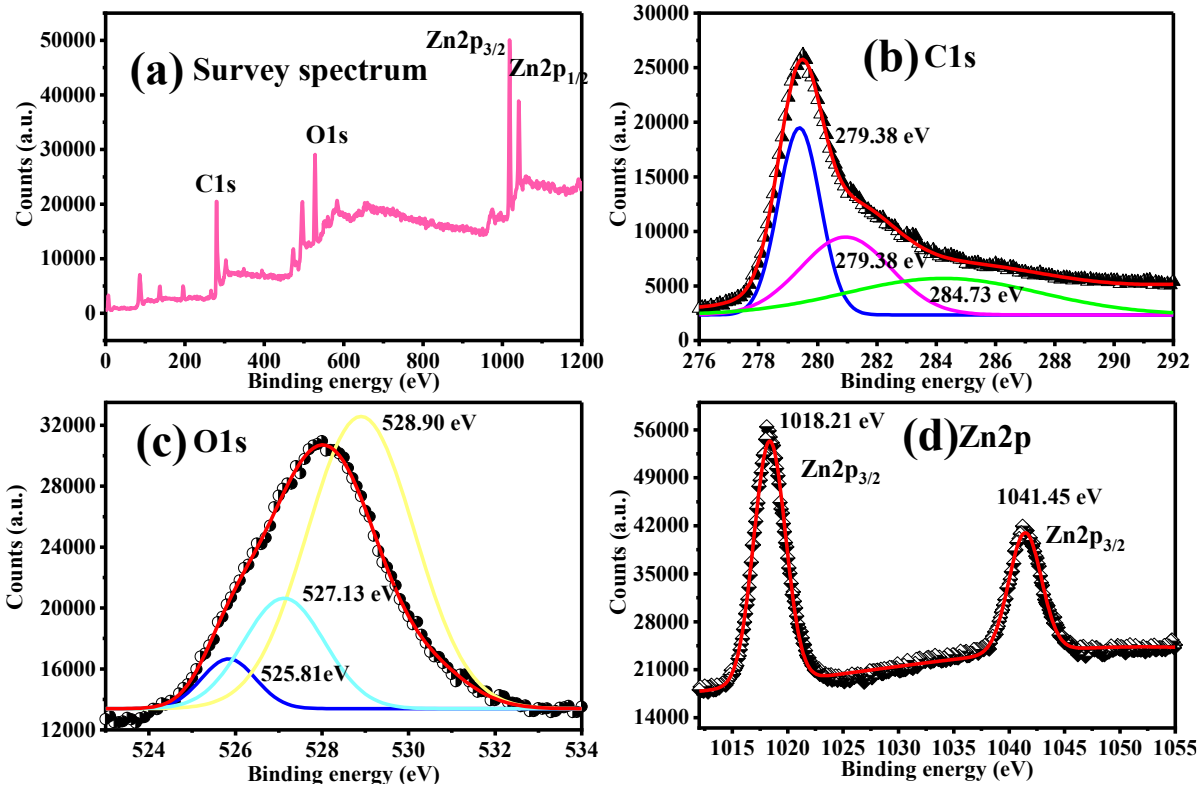

Fig.7.XPS spectra of AC/ZnO nanocomposite

Fig.7 (a) represents the survey spectrum of the AC/ZnO nanocomposite that contains peaks related to Zn, O, and C. The peak observed at 279.50 eV in Fig. 7(b) represents the presence of C1s and confirms the existence of carbon in the +1 oxidation state. Other peaks in the deconvoluted XPS spectra are reported at 280.94 and 284.73 eV, corresponding to the C-O and C-C bonding, respectively. The peak at 528.90 eV in Fig. 7(c) indicates the presence of the O1s state; other peaks observed in the deconvoluted spectrum are reported at binding energy values of 527.13 and 525.81 eV. The XPS peaks corresponding to binding energy values of 1018.21 eV and 1041.45 eV, which can be attributed to Zn2p3/2 and Zn2p1/2, respectively, are shown in Fig. 7(d). The difference of binding energy values between Zn2p3/2 and Zn2p1/2 peaks is ~23 eV, designating the existence of the Zn^{2+} state of Zn in the lattice.

3.1.5. ANALYSIS OF ZETA POTENTIAL CHARACTERISTICS

Zeta potential is a key parameter used to assess the stability of nanomaterials. Nanoparticles with highly positive or highly negative zeta potential values tend to repel each other more strongly, which helps prevent aggregation and allows them to redisperse easily in a medium. Typically, a zeta potential of at least ±30 mV is considered necessary for effective electrostatic and steric stabilization(Lunardi et al., 2020). The AC/ZnO nanocomposite synthesized using the bark of Indian jujube exhibited a zeta potential of +10 mV, suggesting limited stability and moderate dispersibility (Fig.8).

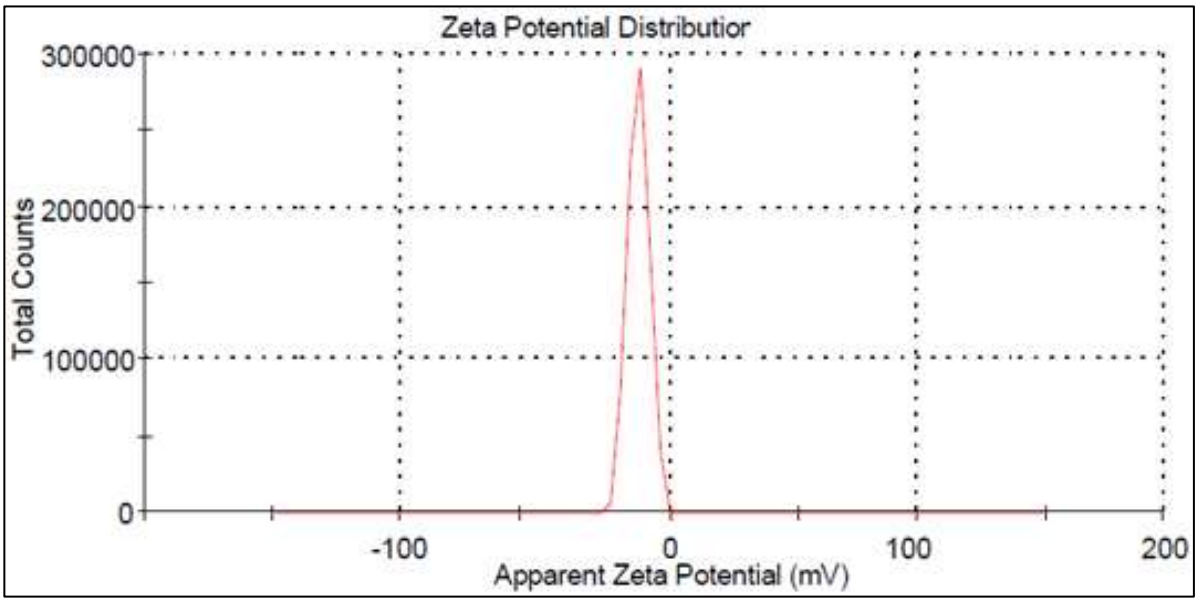

Fig.8. Zeta potential of the prepared AC/ZnO nanocomposite of Indian jujube.

3.1.6. BET ANALYSIS

BET analysis is employed to estimate the pore size, pore volume, and surface area of the synthesized nanoadsorbent. Fig. 9(a) shows the nitrogen (N_2) sorption isotherm of the nanoadsorbent, which corresponds to a Type IV isotherm. The creation of a monolayer is represented by the region that is flat right in the middle. When the pressure is extremely low, the microspores begin to fill with nitrogen gas. At the knee, the creation of monolayers begins, and at medium pressure, the formation of multilayers takes place. Capillary condensation occurs at higher pressures. When the P/P_0 ratio is increased, a greater volume of gas is

adsorbed, indicating that the nanoadsorbent possesses a mesoporous crystal structure (Abdel-Ghani et al., 2019). The surface area of the nanoadsorbent was calculated to be 323.997 m^2/g. According to the BJH approach, which utilizes the Kelvin equation to establish a correlation between pore diameters and pore condensation pressure, the method was employed to calculate the pore size distribution (Fig.9 (d)). With the help of the equation, it was discovered that the average pore volume at 0.255 cc/g and the average pore diameter at 3.15 nm were, respectively.

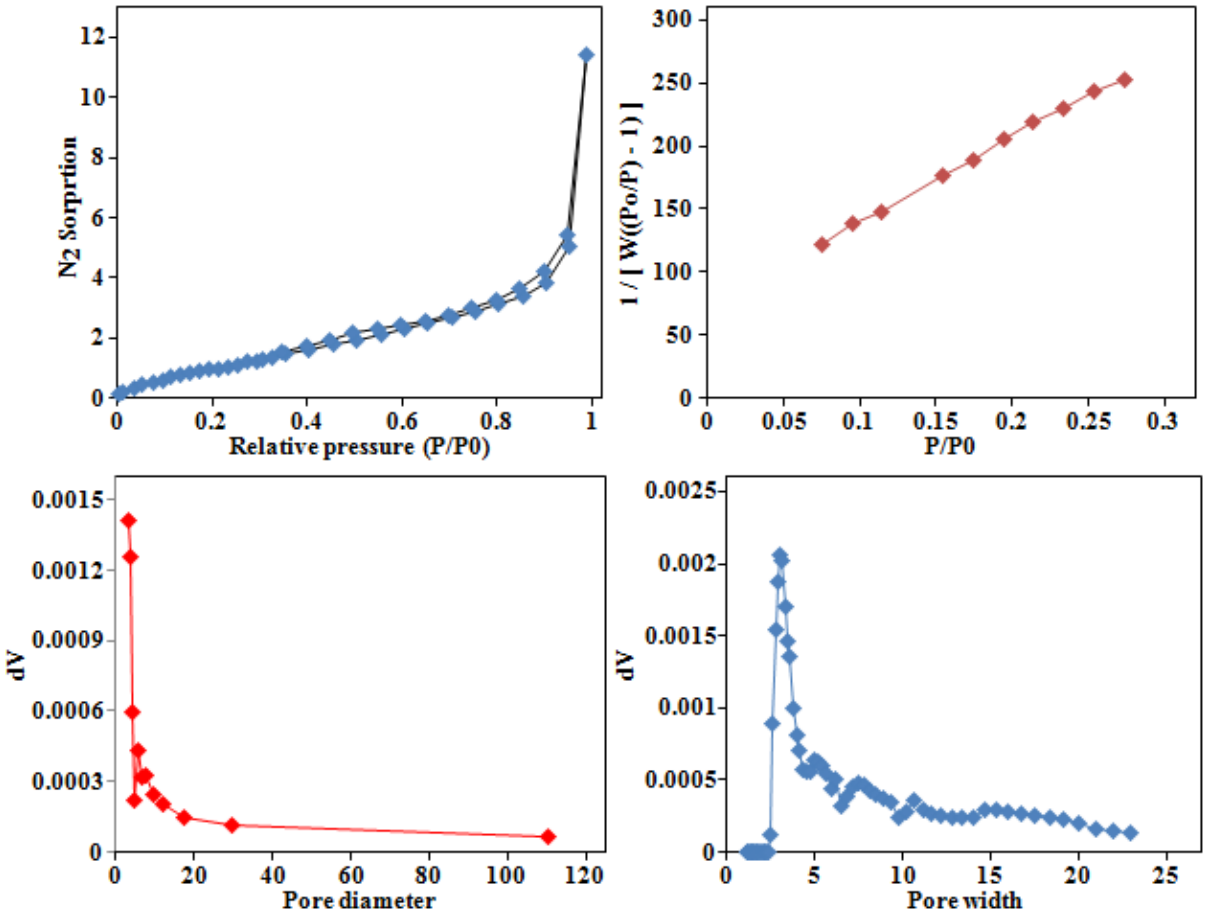

Fig.9 (a) Nitrogen sorption isotherm, (b) BET adsorption isotherm, and BJH pore size distribution curve(c) and (d) of AC/ZnO-nanocomposite synthesized from Indian jujube dead bark

3.2. ADSORPTION PARAMETERS

3.2.1. CONTACT TIME IMPACT

The fluctuation in the adsorption of toluidine dye from the aqueous phase by the nanoadsorbent is depicted in Fig.10, illustrating variations in contact time. Within the first 30 minutes, it is evident that the adsorption process occurred at a rapid pace. Following a period of 60 minutes, the rate of adsorption will equal the rate of desorption. Adsorbing the toluidine blue dye from the aqueous phase in a selective manner was accomplished with the help of the nanoadsorbent that was manufactured. To conduct the adsorption investigation, the time parameter was varied from 10 minutes to 60 minutes. A representation of the adsorption investigation is shown in Fig.10. At an earlier stage, there is a significant acceleration in the adsorption process because the adsorption sites of the nanocomposite that are open for adsorption are not yet occupied. As the vacant sites on the AC-ZnO nanocomposite become occupied by various molecules, the adsorption rate reaches equilibrium with the desorption rate (Naranjo et al., 2023). An equilibrium state is reached when 50 minutes of contact time have passed. Thus, the optimal contact duration for the adsorption investigation currently being conducted is 50 minutes. Because the sorption sites are filled with the molecules of the adsorbate, the adsorption performance does not change after the equilibrium of the adsorption process has been reached. Furthermore, when the contact length was increased from 50 to 60 minutes, no discernible difference in adsorption capability was observed. This was because the adsorbing spots on the nanocomposite surface were saturated.

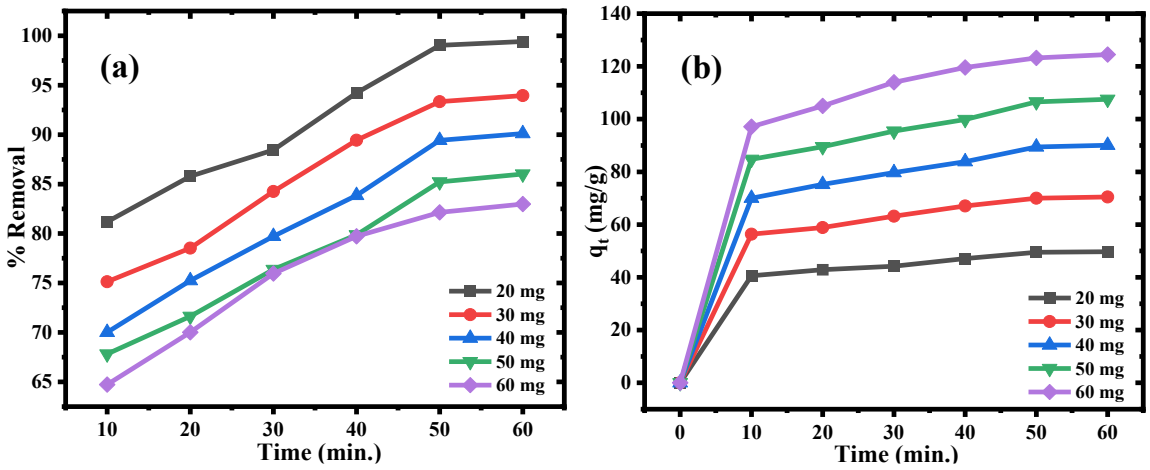

Fig.10. Effect of contact time on the percentage removal efficiency of TB dyes by AC/ZnO nanocomposite.

3.2.2. INITIAL DYE CONCENTRATION IMPACT

An investigation was conducted to examine the effect of varying TB dye concentrations on the adsorption process, with the results presented in Fig. 11(a). The dye concentration was varied from 10 mg/L to 70 mg/L, while maintaining a constant adsorbent dosage of 0.02 g throughout the experiment. The research was conducted at a steady pH level of 11.5. According to the calculations, the percentage of TB dye that was removed dropped from 99.63% to 37.63%. As a result, the dose level of the AC/ZnO nanocomposite was maintained. When there is a lower concentration of dye, there is less occupation of the surface-active sites of the nanocomposite (García, 2018). As a result, there is a greater availability of surface-active sites, which increases the frequency of adsorption. The rate of adsorption is reduced when the accessibility of active sites on the surface is lower, which occurs at higher dye concentrations (A'yuni et. al.2024).

3.2.3. EFFECT OF ADSORBENT DOSE

A more in-depth explanation of how the quantity of adsorbent affects the removal of dye from the aqueous phase (Weber & Morris, 1963) is provided in Fig.11 (b). When the dose of AC/ZnO nanocomposite is increased from 0.02 g to 0.04 g, the percentage of TB dye removed from the solution increases from 86.08% to 99.60%. However, beyond 0.04 g, the adsorption capacity remained relatively stable. This suggests that adsorption was nearly complete with 0.04 g of

the adsorbent and may have been caused by the saturation of empty spaces or the aggregation/agglomeration of adsorbent particles with one another. For further research, 0.02 g of adsorbent was selected. Increasing the adsorbent dose enhances the surface area and number of adsorption sites, while maintaining a consistent dye solution volume and concentration, which may result in improved removal efficiency.

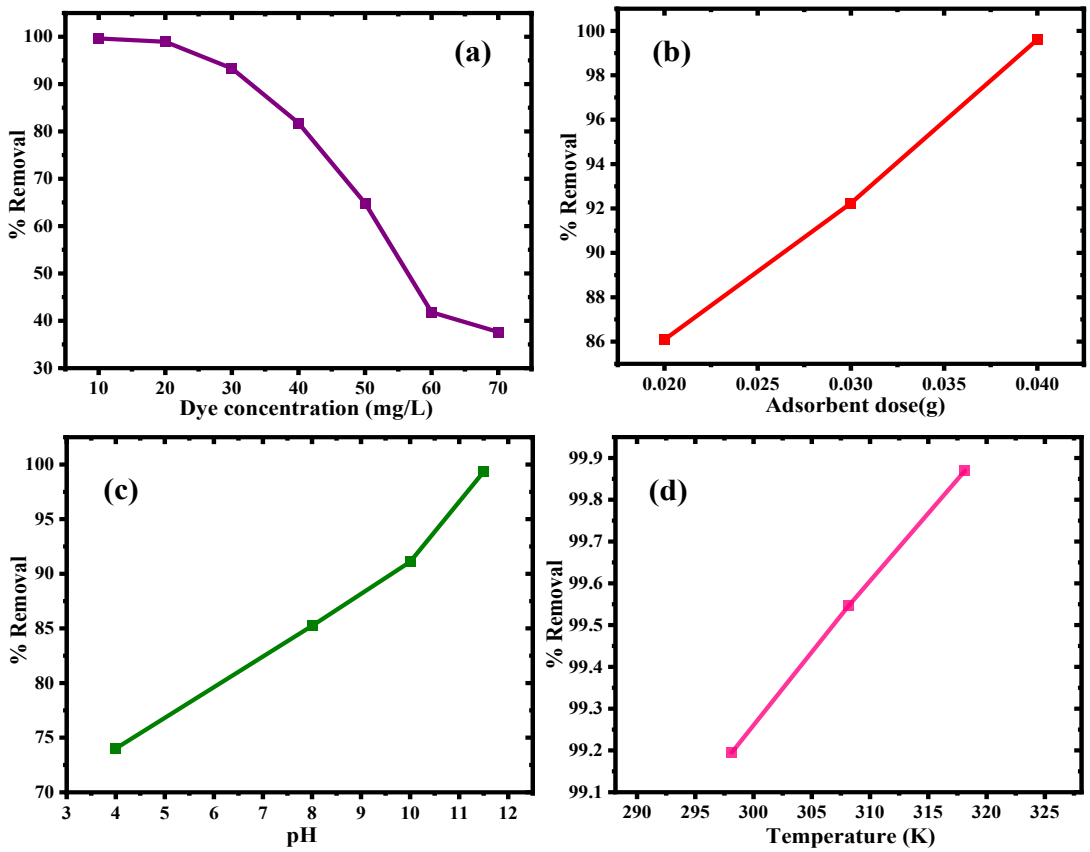

Fig.11 Effect of (a) initial dye concentration, (b) dose amount of nanoadsorbent, (c) pH, and (d) temperature on the percentage removal efficiency of TB dye by AC/ZnO nanocomposite.

3.2.4. pH IMPACT

pH level of the dye solution was adjusted within the range of 4 to 11.5 to investigate its effect on the adsorption of TB onto the AC-ZnO nanocomposite (García, 2018). The results obtained are shown in Fig.11(c), which illustrates the changes in adsorption rates. Based on the data presented in Fig. 11(c), it has been determined that the performance of the nanoadsorbent has improved from 74.01% to 99.33%.

3.2.5. TEMPERATURE IMPACT

The adsorption efficiency of TB dye on the AC/ZnO nanocomposite increased from 99.19% to 99.86% when the temperature of the dye solution was raised to 45 °C. Furthermore, as illustrated in Figure 11(d), the equilibrium adsorption capacity increased from 49.59 mg g^{-1} to 49.93 mg g^{-1}. This improvement is explained by the fact that greater temperatures cause the viscosity of the dye solution to drop, allowing the dye to diffuse more quickly. Additionally, as the temperature rises, the dye's intra-particle diffusion rate also increases, thereby enhancing adsorption (Trivedi et al., 2023). The adsorption process is endothermic if the dye removal trend increases with rising temperature.

3.3. KINETICS STUDY

A kinetic study was conducted to explore the mechanism of TB dye adsorption onto the nanoadsorbent surface from a research perspective. To analyze the adsorption kinetics and underlying mechanism, several kinetic models were applied, including the pseudo-first-order (PFO) (Neme et al., 2022), pseudo-second-order (PSO) (Al-Harby, 2021), Elovich (Al-Harby, 2021), and intra-particle diffusion (IPD) models (Sutherland et. al., 2025). The Elovich model is based on the concept that the solid surface exhibits heterogeneous energy and that the adsorption process becomes slower as more solute is adsorbed (Al-Harby, 2021). In the Elovich kinetic model, the initial adsorption rate is denoted by β (g mg^{-1} min^{-1}), whereas the desorption constant is denoted by α (mg g^{-1} min^{-1}). To compute the values of β and α, it is possible to employ the slope and intercept of the curve that is produced between q_e and ln t. The intra-particle diffusion model (IPD), as described by Weber and Morris (Sutherland et. al., 2025), was employed to identify the rate-determining step.

The constant C (mg g^{-1}) represents the thickness of the boundary layer, while k_{id} (mg g^{-1} $min^{-1/2}$) is the rate constant for the intraparticle diffusion (IPD) kinetic model. By plotting q_t against $t^{0.5}$, the slope and intercept of the resulting graph provide the values of k_{id} and C, along

with the coefficient of determination. If the IPD plot (q_t vs. $t^{0.5}$) yields a straight line passing through the origin with no intercept, it indicates that intra-particle diffusion is the sole rate-controlling step in the adsorption process. Fig.12 presents the kinetic plots for the PFO, PSO, Elovich, and IPD models related to the adsorption of TB dye onto the AC/ZnO nanocomposite synthesized from the bark of Indian jujube. Table 1 summarizes the kinetic parameters for each of the four models. The suitability of these models was evaluated using two key factors: the regression coefficient (R^2) and the closeness between the experimental adsorption capacity (q_e, exp) and the calculated one (q_e, cal).

Among the models, both the PFO and PSO exhibited R^2 values close to unity, indicating a good fit. However, the PSO model showed a better correlation, with R^2 values even closer to 1 and a stronger agreement between q_e, exp, and q_e, cal across all TB dye concentrations tested. This suggests that the PSO kinetic model provides a more accurate representation of the adsorption behaviour of TB dye on the AC/ZnO nanocomposite. It is also more effective in predicting parameters related to adsorb mass, surface diffusion, and activation/deactivation energies. In addition, the Elovich model also provided a reasonable fit to the experimental data, indicating that chemisorption plays a role in the adsorption process. The higher values of α compared to β in the Elovich model further support the observation that adsorption is more favorable than desorption in this system.

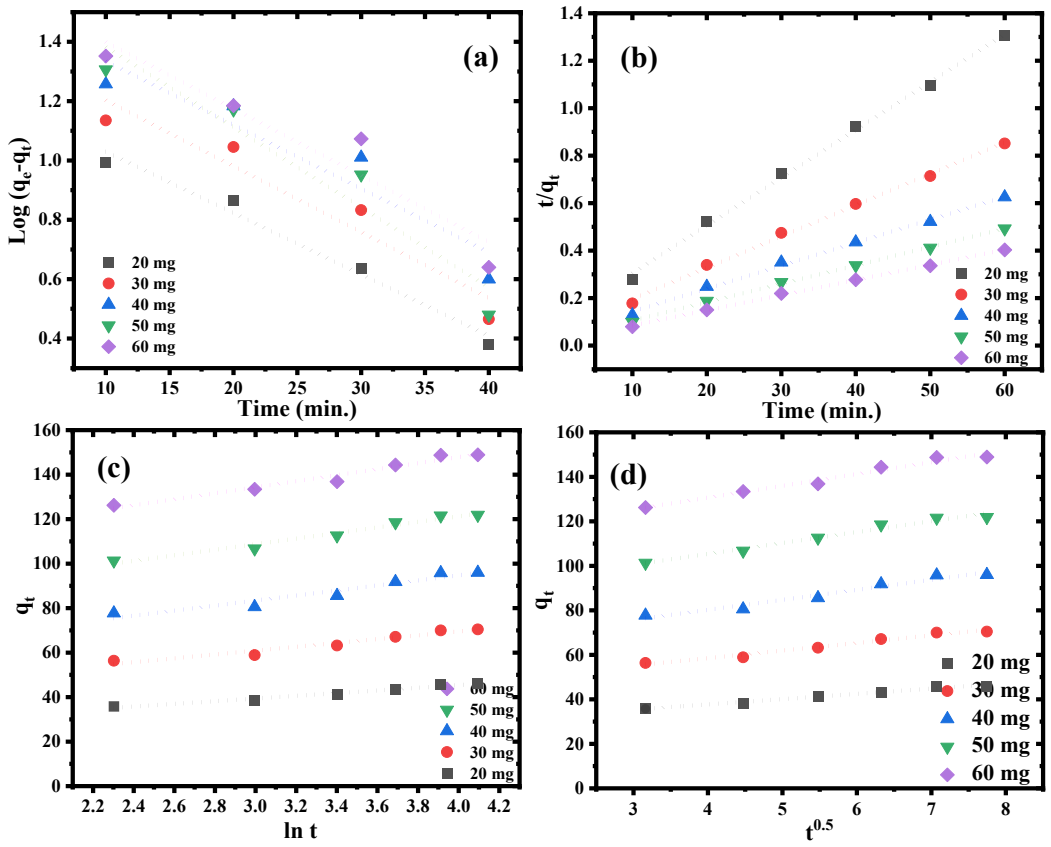

Fig.12. Depicting (a) pseudo first order, (b) pseudo second order, (c) Elovich (d) intra-particle diffusion kinetics for TB dye adsorption by AC/ZnO nanocomposite.

Table 1: The AC/ZnO nanocomposite's kinetic characteristics for TB dye adsorption.

Kinetics Models	**Parameters**	**Dye Concentration**				
		20 mg	**30 mg**	**40 mg**	**50 mg**	**60 mg**
First order	q_e, exp (mg g^{-1})	17.206	26.67	35.463	44.951	42.161
	K_1 (min^{-1})	0.0476	0.0512	0.0494	0.0622	0.05184
	q_e, cal (mg g^{-1})	49.514	70	89.433	106.53	123.22
	R	0.99	0.963	0.942	0.962	0.955
Second order	q_e, cal (mg g^{-1})	49.652	75.816	103.306	129.032	156.495
	K_2 (g mg^{-1} min^{-1})	0.004	0.003	0.002	0.002	0.002
	R	0.999	0.999	0.999	0.999	0.999

Elovich	β	0.165	0.116	0.088	0.079	0.074
	α	204.96	503.83	875.62	3659.31	13950.92
	R	0.986	0.974	0.962	0.985	0.981
Intraparticle	K_{id}	2.368	3.406	4.509	4.897	5.303
	C	28.253	44.887	62.174	85.792	109.47
	R	0.993	0.988	0.988	0.988	0.988

Moreover, the presence of nonzero intercepts in the IPD model plots, along with R^2 values significantly lower than unity, suggests that intra-particle diffusion is likely not the primary rate-controlling step in the adsorption process (Sutherland et. al., 2025). As a result, the R^2 values deviate from unity.

3.4. ADSORPTION EQUILIBRIUM STUDIES

Adsorption equilibrium studies are crucial in the context of removing dyes from aqueous solutions using nanoadsorbents. These studies are used to gain knowledge of the interaction that occurs between the dye molecules and the nanoadsorbent composition. Adsorption equilibrium studies often involve the use of adsorption isotherms to describe the relationship between the amount of dye adsorbed onto the nanoadsorbent before equilibrium and the concentration of dye remaining in the wastewater. One of the assumptions made by the Langmuir isotherm model is that monolayer adsorption occurs on a surface that is homogeneous and has a finite number of adsorption sites that are similar and have the same energy (Sangon et al., 2020). To predict the adsorption capacity of the nanoadsorbent as well as the equilibrium constant that is associated with adsorption energy, the Langmuir equation can be utilized. The separation factor (R_L) can be used to determine whether the adsorption process is advantageous. When R_L is more than 1, the process is known to be unfavourable; when R_L is equal to 1, the process is considered to be linearly favourable; when R_L is between

0 and 1, the process is supposed to be advantageous; and when R_L is equal to zero, the process is considered to be irreversible.

The Freundlich isotherm model (Neme et al., 2022) is an empirical approach used to describe multilayer adsorption on heterogeneous surfaces (Sajjadi &Goharshadi, 2017). According to this hypothesis, the adsorption energy is likely to decrease as the surface coverage rises. The adsorption capacity and intensity of the nanoadsorbent can be evaluated using the Freundlich equation.These isotherm models characterize the adsorption process using key parameters, including the equilibrium concentration of the dye in the solution (C_e) and the amount of dye adsorbed on the nanoadsorbent at equilibrium (q_e). The Temkin isotherm is based on a relationship between the coverage of the adsorbent surface by the adsorbate and the heat released during the adsorption process. The isotherm says that as the surface of the adsorbent gets covered, the heat of sorption decreases.

The Dubinin-Radushkevich adsorption isotherm helps determine the kind of adsorption, whether it is physisorption or chemisorption, and also calculates the energy of adsorption. In adsorption equilibrium investigations, the correlation coefficients (R^2 values) generated by fitting experimental data to the various isotherm models are utilized to determine the degree to which these models accurately describe the real behaviour of adsorption (Fig.13). Higher R^2 values suggest that the model is a better fit for the data obtained through experimentation. Researchers can gain insights into the adsorption mechanisms, capacity, and effectiveness of nanoadsorbents in removing dyes from wastewater by conducting adsorption equilibrium studies using nanoadsorbents and analyzing the data using different isotherm models. The linear equations and the respective constants obtained for each model are presented in Table 2. Based on the R^2 values and isotherm constants, it is evident that the Langmuir model best fits the experimental data, indicating a monolayer adsorption process. The Freundlich and the D-R models also showed strong applicability, suggesting surface heterogeneity. Although the

Temkin model contributed additional understanding of the adsorption energy and interactions, their lower R^2 values suggest limited suitability for this system.

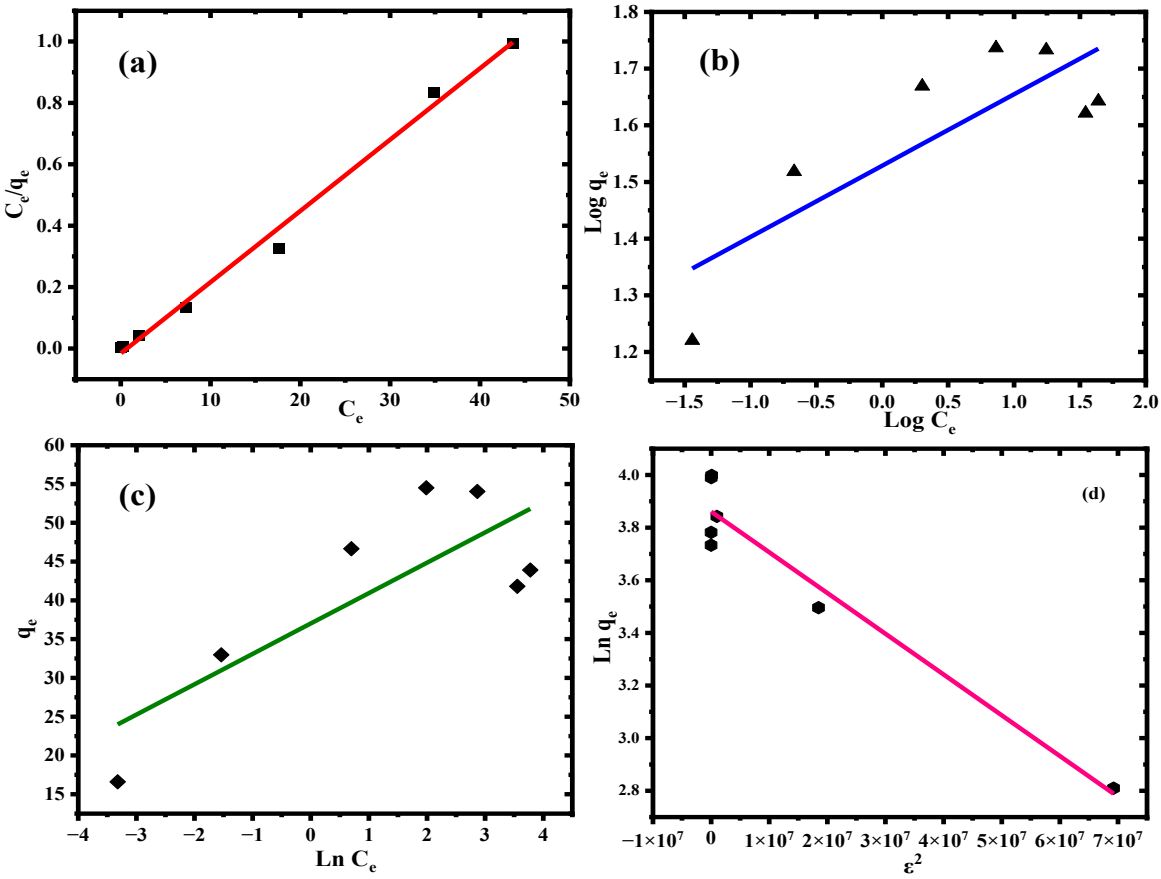

Fig.13. (a) Langmuir isotherm, (b) Freundlich isotherm, (c) Temkin isotherm, and (d) Dubinin–Radushkevich isotherm plots representing the adsorption of TB dye onto the synthesized AC/ZnO nanocomposite.

Table 2: Isotherm parameters for removing TB dye over AC/ZnO nanocomposite.

		Values of isotherm
Isotherms	**Paramerers**	**parameters**
Langmuir	q_{max} (mg g^{-1})	84.034
	b_L (L mg^{-1})	8.207
	R_L	0.012
	R^2	0.999

Freundlich	K_f (mg g^{-1})(L mg^{-1})$^{1/n}$	140.142
	N	2.488
	R^2	0.9904
Tempkin	b_T	579.74
	K_T (L $g^{-1)}$	1.26 x 10^4
	B_T (J mol^{-1})	3.9172
	R^2	0.75939
D-R	K_{id} (mol^2 kJ^{-2})	1.54 x 10^{-8}
	E	5.68 x 10^3
	R^2	0.936

3.5. THERMODYNAMIC STUDY OF ADSORPTION

To gain a better understanding of the practicability and effectiveness of the process, it is essential to research the thermodynamics of adsorption for removing colours from aqueous solutions using nanoadsorbents. The following parameters can be taken to determine the spontaneity of adsorption on the surface of nanoadsorbents. Gibbs free energy (Al-Kadhi, 2019), the enthalpy (Badran & Khalaf, 2020), and the entropy. Since the adsorption is spontaneous, $\Delta G^{\circ}<0$, adsorption, on the other hand, is not a spontaneous process. Any ΔS° that is positive indicates an increased disorder (Mahvelati-Shamsabadi et al., 2018). When ΔS° is negative, it means a reduction in disorder.

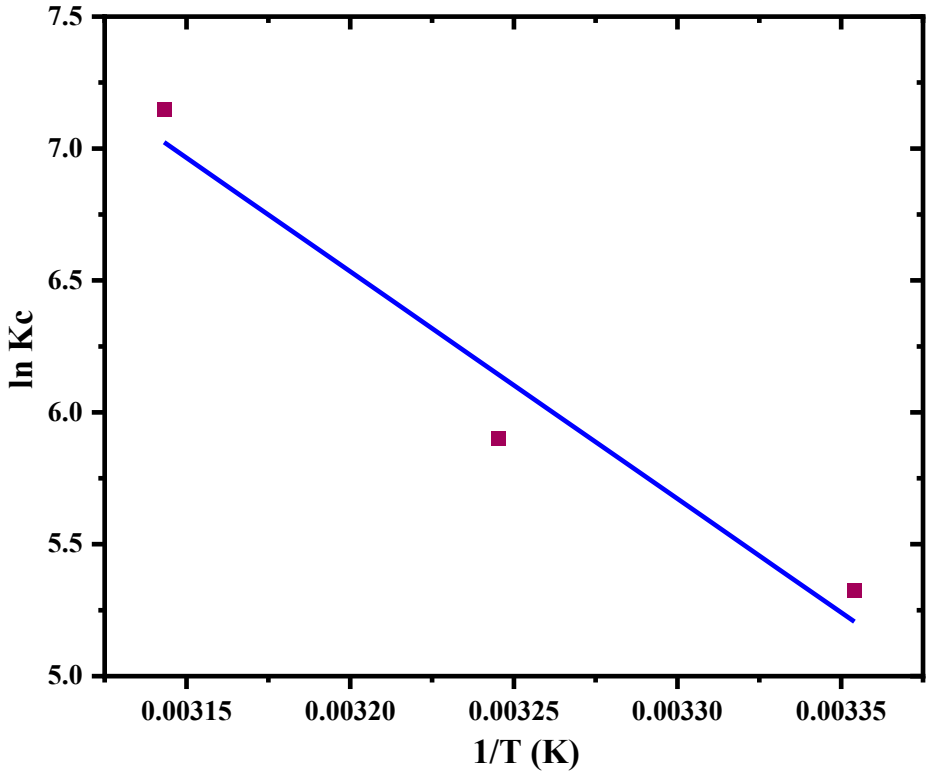

Fig. 14: Correlation between temperature and the equilibrium constant (K_c) for the adsorption of TB dye on the AC/ZnO nanocomposite.

Based on the plot of ln K_c versus 1/T depicted in Fig.14, the slope and intercept were employed to determine the ΔH° and ΔS° values, respectively. A detailed summary of these thermodynamic parameters is provided in Table 3. The negative values of ΔG° confirm the spontaneous nature of the adsorption process, indicating its thermodynamic favorability. The ΔG° values range from –22 to 0 kJ/mol, consistent with the characteristics of chemisorption. Moreover, the positive enthalpy change (ΔH° = 71.64 kJ/mol) indicates that the adsorption is endothermic and primarily physical, as values exceeding 40 kJ/mol typically suggest physisorption. The positive entropy change (ΔS° = 262.946 J/mol·K) further reinforces this, indicating increased randomness at the solid–liquid interface during the adsorption process.

Table 3: Thermodynamic parameters associated with TB dye adsorption on AC/ZnO nanocomposite.

Temperature	ΔG° (kJ mol^{-1})	ΔH° (kJ mol^{-1})	ΔS° (J mol^{-1} K^{-1})
298.15	-16.05		
308.15	-17.76	71.64	262.946
318.15	-21.35		

3.6. RECYCLABILITY OF THE ADSORPTION PROCESS

To eliminate TB dye from water, AC/ZnO nanocomposite made from the dead bark of the Indian jujube (*Ziziphus mauritiana*) was utilized as the adsorbent. Throughout four successive cycles, the adsorption and regeneration processes were carried out on the nanocomposite (Mahto et al., 2014). Following each cycle of adsorption, the adsorbent was recovered by centrifugation, rinsed with water and alcohol to remove the TB dye that had been adsorbed, and then dried at 85°C for 4 hours. The efficiency of eliminating TB dye remained consistent throughout all four cycles, with the fourth cycle exhibiting an efficiency of approximately 90.1% removal (Fig.15). By measuring the FTIR spectrum of the AC/ZnO nanocomposite that was utilized, it was possible to confirm that the TB dye removal process was successful (Fig.16). Following the adsorption of TB dye, the peaks in the FTIR spectra that were related to the functional groups of the prepared nanocomposite moved to higher wave numbers within the spectrum. These peaks exhibited a decrease in strength, indicating a connection between the aromatic structures of the AC/ZnO nanocomposite and the benzene ring of the TB molecules. This interaction is likely to be a π–π interaction. The stability and efficiency of the AC/ZnO nanocomposite as an adsorbent are suggested by the fact that it has an AC performance that is consistent across several cycles. In practical applications, where adsorbents need to be reused multiple times without significant loss of efficiency, this is a crucial consideration. To successfully recover the adsorption ability of AC/ZnO nanocomposite prepared by the dead bark of Indian jujube (Ziziphus mauritiana), the regeneration procedure

outlined (which included centrifugation, washing, and drying) was utilized. This made the material appropriate for ongoing usage. The evidence of TB dye adsorption onto AC-ZnO nanocomposite prepared by Indian jujube (Ziziphus mauritiana) bark is provided by the shift in FTIR peaks and the decrease in intensity. This confirms the mechanism of adsorption through π–π interactions.

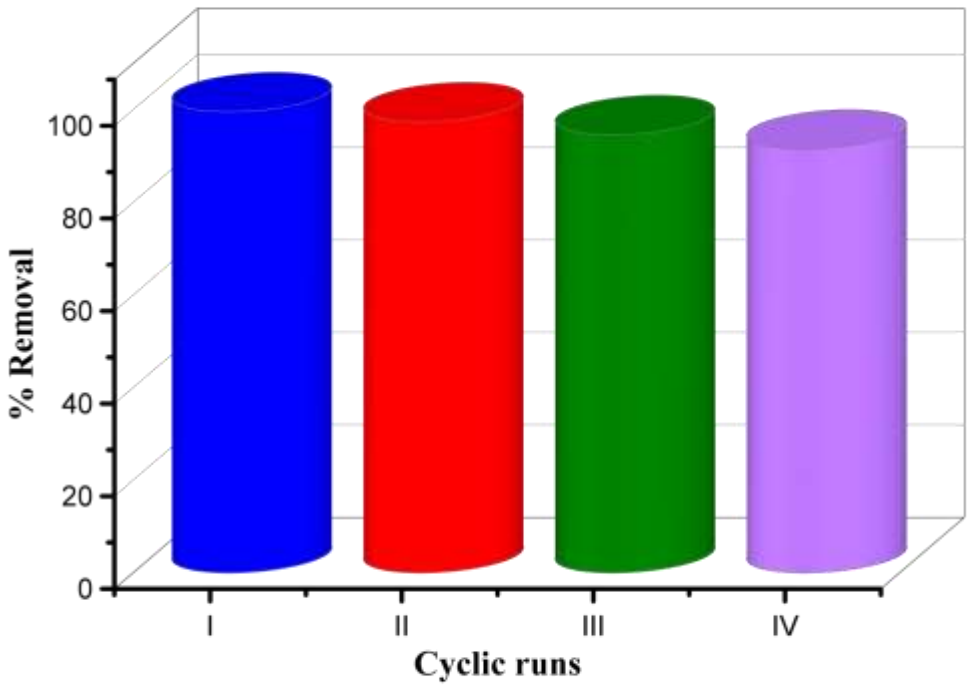

Fig.15. Recyclability of AC/ZnO nanocomposite prepared from dead bark of Indian Jujube

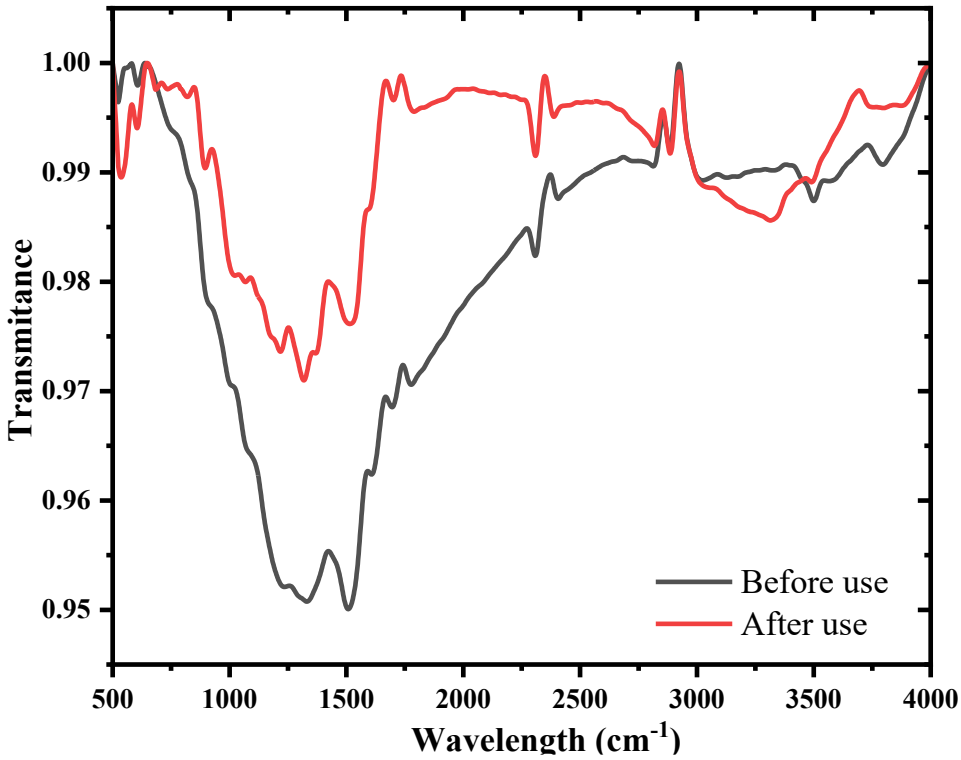

Fig.16.FTIR before and after the adsorption of TB dye by AC/ZnO nanocomposite.

In conclusion, the research reveals that the AC/ZnO nanocomposite prepared from the dead bark of the Indian jujube is a stable and recyclable material that may be used as an adsorbent for removing TB dye from wastewater. The discovery of such results is crucial for the development of water treatment methods that are both environmentally benign and economically feasible, utilizing natural and renewable adsorbents.

Table 4: Comparison of the adsorption efficiency of the Indian jujube

Adsorbent	Pollutant	Contact time (min)	% Removal	References
H_3PO_4 Activated Indian jujube seeds	AF	60	94.68%	(Bouchelkia et al. 2023)
	TB		92.42%	
Jujube Cores	MB	120	95%	(Malika et al. 2021)
	MO		93.87%	

	MB	150	89.50%	(Venkatesan et al. 2024)
FeNP-Jujube leaf extract AC/ZnO nanocomposite from the bark of Indian jujube	TB	50	99.60%	**Present study**

4. CONCLUSION

The present work demonstrates the successful synthesis of an activated carbon/zinc oxide (AC/ZnO) nanocomposite from the dead bark of Ziziphus mauritiana and its application in the removal of toluidine blue dye from water. Structural and surface analyses confirmed the formation of a porous nanocomposite with uniform ZnO dispersion. Batch adsorption studies revealed that the optimal conditions for TB dye removal were 0.04 g of adsorbent in 100 mL of solution at pH 11.5, contact time 50 minutes, and room temperature, under which 99.6% removal was achieved with a maximum adsorption capacity of 49.9 mg g^{-1}. The adsorption process obeyed the Langmuir isotherm and pseudo-second-order kinetics, suggesting monolayer chemisorption as the dominant mechanism. Thermodynamic analysis confirmed spontaneity and endothermic nature of the adsorption process. The adsorbent exhibited excellent recyclability, maintaining >90% removal efficiency after four successive cycles.

This study highlights the novelty of utilizing Z. mauritiana bark, an underexplored and abundantly available biomass, as a precursor for producing efficient AC/ZnO nanocomposites. While the results demonstrate high removal efficiency and reusability, further studies on multi-component dye systems and Zn-leaching assessment are necessary before field-scale applications. Overall, the work provides a sustainable and low-cost pathway for developing nanocomposite adsorbents for wastewater remediation.

Conflicts of Interest

The authors declare that they have no conflicts of interest concerning the research described in this manuscript.

Financial Interest

The authors confirm that they have no relevant financial or non-financial interests related to this work.

Acknowledgment

The authors express their sincere gratitude to the Department of Chemistry, University of Rajasthan, Jaipur, for providing the necessary facilities to conduct this research.

REFERENCES

1) A'yuni, D. Q., Hadiantono, H., Velny, V., Subagio, A., Djaeni, M., Mufti, N., 2024. Effect of Potassium Hydroxide Concentration and Activation Time on Rice Husk-Activated Carbon for Water Vapor Adsorption. Iranian Journal of Materials Science and Engineering. 21 (3), pp. 1-10. http://doi.org/10.22068/ijmse.3522

2) Abdel-Ghani, N. T., El-Chaghaby, G. A., Rawash, E. A., and Lima, E. C., 2018. Magnetic activated carbon nanocomposite from Nigella sativa L. waste (MNSA) for the removal of Coomassie brilliant blue dye from aqueous solution: statistical design of experiments for optimization of the adsorption conditions. J. Adv. Res. 17, pp. 55–63. https://doi.org/10.1016/j.jare.2018.12.004

3) Abo El Naga, A.O., Saied, M. E., Shaban, S. A., and Kady, F. Y. E., 2019. Fast removal of diclofenac sodium from aqueous solution using sugar cane bagasse-derived activated carbon. J. Mol. Liq. 285, pp. 9–19. https://doi.org/10.1016/j.molliq.2019.04.062

4) Agrawal, M., Maheshwari, K., and Solanki, Y. S., 2021. Investigation of Dye Effluent Treatment Using Unmodified and Modified Biobased Sorbent and Its Process Economics. Journal of Hazardous, Toxic, and Radioactive Waste. 26(1). https://doi.org/10.1061/(ASCE)HZ.2153-5515.0000650

5) Ahmad, A., Khan, N., Giri, B., Chowdhary, P., and Chaturvedi, P., 2020. Removal of methylene blue dye using rice husk, cow dung, and sludge biochar: characterization, application, and kinetic studies. Biores. Technol., 306, 123202. pp. 1-5. https://doi.org/10.1016/j.biortech.2020.123202

6) Ahmad, A., Mohd-Setapara, S. H., Chuong, C. S., Khatoona, A., Wani, W. A., Kumar, R,. and Rafatullah, M., 2015. Recent Advances in New Generation Dye Removal Technologies: Novel Search of Approaches to Reprocess Waste Water. RSC adv.5, pp. 30801-30818. https://doi.org/10.1039/C4RA16959J

7) Akhtar, M., Sarfaraz, M., Ahmad M., Raza, N., Zhang, L. 2025. Use of low-cost adsorbent for waste water treatment: Recent progress, new trend and future perspectives. Desalination and Water treatment, 321, pp. 100914. https://doi.org/10.1016/j.dwt.2024.100914

8) Al-Harby, N. F., Albahly, E. F., Mohamed, N. A. 2021. Kinetics, Isotherm and Thermodynamic Studies for Efficient Adsorption of Congo Red Dye from Aqueous Solution onto Novel Cyanoguanidine-Modified Chitosan Adsorbent. Polymers (Basel). 13 (24), pp. 4446. https://doi.org/10.3390/polym13244446

9) Al-Kadhi, N. S., 2019. The kinetic and thermodynamic study of the adsorption of Lissamine green B dye by micro-particles of wild plants from aqueous solutions. Egypt. J. Aquat. Res., 45 (3), pp. 231–238. https://doi.org/10.1016/j.ejar.2019.05.004

10) Badran, I., and Khalaf, R., 2019. Adsorptive removal of alizarin dye from wastewater using maghemite nanoadsorbents. Sep. Sci. Technol., 55(5), pp. 1-16. https:// doi.org/10. 1080/01496395.2019.1634731

11) Bouchelkia, N., Benazouz, B., Mameri, A., Belkhiri, L., Hamri, N., Belkacemi, H., Zoukel, A., Amrane, A., Aoulmi, F., and Mouni, L., 2023. Study and Characterization of H3PO4 Activated Carbons Prepared from Jujube Stones for the Treatment of Industrial Textile Effluents. Processes. 11(9), 2694. pp. 1-19. https://doi.org/10.3390/pr11092694

12) Deshmukh, S., Topare, N. S., Raut-Jadhav, S., Thorat, P. V., Bokil, S. A., Khan, A. 2022. Orange peel activated carbon produced from waste orange peels for adsorption of methyl red. AQUA - Water Infrastructure, Ecosystems and Society. 71 (12), pp. 1351–1363. https://doi.org/10.2166/aqua.2022.119

13) El maguana, Y., Elhadiri, N., Benchanaa, M., and Chikri, R., 2020. Activated carbon for dyes removal: modeling and understanding the adsorption process. J. Chem. 209683, pp 1-9. https://doi.org/10.1155/ 2020/2096834.

14) Feng, P., Li, J., Wang, H., and Xu, Z., 2020 Biomass-Based Activated Carbon and Activators: Preparation of Activated Carbon from Corncob by Chemical Activation with Biomass Pyrolysis Liquids. ACS Omega. 5 (37). pp. 24064-24072 https://doi.org/10.1021/acsomega.0c03494

15) Ghaedi, M., Sadeghian, B., Pebdani, A. A., Sahraei, R., Daneshfar, A., and Duran, C., 2012. Kinetics, thermodynamics and equilibrium evaluation of direct yellow 12 removal by adsorption onto silver nanoparticle-loaded activated carbon. Chem. Eng. J. 187, pp. 133–141. https://doi.org/10.1016/j.cej.2012.01.111

16) González-García, P., 2018. Activated carbon from lignocellulosic precursors: a review of the synthesis methods, characterization techniques, and applications. Renew. Sustain. Energy Rev. 82 (1), pp. 1393–1414. https://doi.org/10.1016/j.rser.2017.04.117

17) Gupta, S. S., Kausor, M. A., Chakrabortty, D., 2025. Banana peel as potential bioadsorbent toward removal of emerging contaminants from wastewater for sustainable environment: a review.,Chemical Papers., 79, pp. 2717-2750. https://doi.org/10.1007/s11696-025-03945-5

18) Hambisa, A. A., Regasa, M. B., Ejigu, H.G., and Senbeto, C. B., 2022. Adsorption studies of methyl orange dye removal from aqueous solution using Anchote peel-based agricultural waste adsorbent. Appl. Water Sci. 13(24), pp. 1–11. https://doi.org/10.1007/s13201-022-01832-y

19) Hansima, M. A. C. K., Makehelwala, M., Jinadasa, K. B. S. N., Wei, Y., Nanayakkara, K. G. N., Herath, A. C., and Weerasooriya, R., 2021. Fouling of ion exchange membranes used in the electrodialysis reversal advanced water treatment: A review. Chemosphere. 263, 127951. https://doi.org/10.1016/j.chemosphere.2020.127951

20) Hu, Q., Hao, L. 2025. Adsorption Technologies in Wastewater Treatment Processes. Water. 17(15), pp. 2335. https://doi.org/10.3390/w17152335

21) Jani, Y., 2022. Adsorption: A Cost-Effective Wastewater Treatment Technology for Removal of Conventional and Emerging Organic Contaminants. Cost-efficient Waste Water Treatment Technologies, pp. 17-33.

22) Khazaal, M. H., Khalaf, Z. A., 2022. A Comprehensive Review of Wastewater Treatment Using Adsorption Process onto Low-Cost Adsorbents. HIV Nursing, 22 (2). pp. 1081-1087.

23) Lunardi, C. N., Gomes, A. J., Rocha, F.S., Tommaso, J. D., and Patience, G. S., 2020. Experimental methods in chemical engineering: Zeta potential. Can J Chem Eng. 99, pp. 627–639. https://doi.org/10.1002/cjce.23914

24) Luo, L., Wu, X., Li, Z., Zhou, Y., Chen, T., Fan, M., and Zhao, W., 2019. Synthesis of activated carbon from biowaste of fir bark for methylene blue removal. R. Soc. Open Sci. 6, 190523 p. 1-14. http://dx.doi.org/10.1098/rsos.190523

25) Mahto, T. K., Chowdhuri, A. R., Sahu, S. K., 2014. Polyaniline-functionalized magnetic nanoparticles for the removal of toxic dye from wastewater. J. Appl. Polym. Sci. 40840. pp. 1-9. https://doi.org/ 10. 1002/app.40840

26) Mahvelati-Shamsabadi, T., Goharshadi, E. K., Shafaee, M., Niazi, Z., 2018. ZnS@ reduced graphene oxide nanocomposite as an effective sunlight-driven photocatalyst for degradation of reactive black 5: A mechanistic approach. Sep. Purif. Technol. 202, pp.326-334. https://doi.org/10.1016/j.seppur.2018.04.001

27) Malika, M., Belaid, Dra, R. E. A., Boumediane, I., Soundess, and Khadidja, G., 2021. Activated carbon from jujube cores for removal of cationic dyes from wastewater. Journal of Materials and Structures. 06, pp. 01–12.

28) Mordhiya, B., Sharma, R., Meena, P. L., and Meena, P., 2024. Development of novel adsorbent for removal of organic contaminants from polluted water: kinetic, isotherm, and thermodynamic studies. J IRAN CHEM SOC. 21, pp. 835–851. https://doi.org/10.1007/s13738-023-02964-x

29) Naranjo, J., Juiña, E., Loyo, C., Romero, M., Vizuete, K., Debut, A., Ponce, S., Murillo, H. A. 2023. Preparation of Adsorbent Materials from Rice Husk via Hydrothermal Carbonization: Optimization of Operating Conditions and Alkali Activation. Resources. 12 (12), 145, https://doi.org/10.3390/resources12120145

30) Nath, I., Chakraborty, J., Heynderickx, P. M., and Verpoort, F., 2018. Engineered synthesis of hierarchical porous organic polymers for visible light and natural sunlight induced rapid degradation of azo, thiazine, and fluorescein-based dyes in a unique mechanistic pathway. Appl. Catal., B 227, pp. 102–113. https://doi.org/10.1016/j.apcatb.2018.01.032

31) Neme, I., Girma, G., and Chandran, M., 2022. Activated carbon from biomass precursors using phosphoric acid: A review. Heliyon. 12: e11940. https://doi.org/10.1016/j.heliyon.2022.e11940

32) Nguyena, C. H., Tranb, H. N., Fu, C. C., Lu, Y. T., and Juang, R. S., 2020. Roles of adsorption and photocatalysis in removing organic pollutants from water by activated carbon-supported. Journal of the Taiwan Institute of Chemical Engineers, 109, pp. 51-61. https://doi.org/10.1016/j.jtice.2020.02.019

33) Omri, A., Benzina, M., 2012. Characterization of activated carbon prepared from a new raw lignocellulosic material: Ziziphus spina-christi seeds. J. Soc. Chim. Tunis, 14, pp.175–183.

34) Sajjadi, S. H., and Goharshadi, E. K., 2017. Highly monodispersed hematite cubes for removal of ionic dyes. J. Environ. Chem. Eng. 5, pp. 1096– 1106. https://doi.org/10.1016/j.jece.2017.01.035

35) Sangon, S., Hunt, A. J., Attard, T. M., Mengchang, P., and Supan-chaiyamat, N., 2018. Valorisation of waste rice straw for the production of highly effective carbon-based adsorbents for dyes removal. J. Clean. Production. 172, pp. 1128-1139. https://doi.org/10.1016/j.jclepro.2017.10.210

36) Shrivastva R., Singh N. K., 2022. Agro-wastes sustainable materials for wastewater treatment: Review of current scenario and approaches for India. *Materials today proceedings.* 60 (1), pp. 552-558. https://doi.org/10.1016/j.matpr.2022.01.460

37) Sulaiman, S., Azis, R. S., Ismail, I., Man, F. C., Yusof, K. F. M., Abba, M. U., and Katibi, K. K., 2021. Adsorptive Removal of Copper (II) Ions from Aqueous Solution Using a Magnetite Nano-Adsorbent from Mill Scale Waste: Synthesis, Characterization, Adsorption and Kinetic Modelling Studies. *Nanoscale Res Lett. 16 (1), 168.* https://doi.org/10.1186/s11671-021-03622-y

38) Sutherland, C., 2025. A method of classifying the influence of intraparticle diffusion in adsorption systems: characteristic curves of the diffusion-chemisorption kinetic model. Environmental Toxicology and Chemistry. 44 (5) pp. 1209-1221. https://doi.org/10.1093/etojnl/vgaf052

39) Tripathi, N., 2013. Cationic and anionic dye adsorption by agricultural solid wastes; a comprehensive review. *Journal of Applied Chemistry*. 5 (3), pp. 91-108.

40) Trivedi, Y., Sharma, M., Sharma, A., 2023. Surface modification of mustard husk char to enhance its adsorption properties. Materials Today Proceedings, 76 (1), pp. 29-35. https://doi.org/10.1016/j.matpr.2022.08.391

41) Venkatesan, G., Koteshwaran, S., Rengasamy, M., Rajeshkannan, R., Saravanan, V., Sujatha, S., Saravanan, P., and Rajasimman, M., 2024. Efficient removal of methylene blue dye by iron nanoparticles synthesized by a novel green method using jujube leaf extract: characterization, kinetics, and isotherm studies. *Biomass Conversion and Biorefinery.* 14, pp. 29433-29449. https://doi.org/10.1007/s13399-023-05071-2

42) Yadav, A., Bagotia, N., Yadav, S., Sharma, A.K., and Kumar, S. 2021. Adsorptive studies on the removal of dyes from single and binary systems using Saccharum munja plant-based

novel functionalized CNT composites. *Environ. Technol. Innov.* 24, 102015. pp. 1-14 https://doi.org/10.1016/j.eti.2021.102015